



An equivalent soil mechanics formulation for rigid wheels in deformable terrain, with application to planetary exploration rovers

H. Shibly^a, K. Iagnemma^{b,*}, S. Dubowsky^b

^a *Mechanical Engineering Department, Birzeit University, Palestinian Territories, via Israel*

^b *Mechanical Engineering Department, Massachusetts Institute of Technology, Cambridge, MA 02139, USA*

Available online 1 July 2004

Abstract

A simplified, closed-form version of the basic mechanics of a driven rigid wheel on low-cohesion deformable terrain is presented. This approach allows the formulation of an on-line terrain parameter estimation algorithm, which has important applications for planetary exploration rovers. Analytical comparisons of the original and simplified equations are presented, and are shown to closely agree. Experimental results from a single-wheel testbed operating in dry sand shows that the simplified equations can be used for mobility prediction with good accuracy. Methods for incorporating the simplified equations into an on-line terrain parameter algorithm are discussed.

© 2004 ISTVS. Published by Elsevier Ltd. All rights reserved.

Keywords: Rigid wheel mechanics; Deformable terrain; Mobility prediction; Planetary rovers

1. Introduction and related research

During future planetary exploration missions, wheeled mobile robots (“rovers”) will be required to negotiate rough-terrain of varying composition [1]. It is well known that wheel–terrain interaction plays a critical role in rough-terrain vehicle mobility [2]. Knowledge of terrain parameters, such as cohesion and internal friction

* Corresponding author. Fax: +1-617-253-9637.

E-mail address: kdi@mit.edu (K. Iagnemma).

angle, would lead to improved prediction of wheel–terrain interaction mechanics, which would allow rovers to perform important scientific tasks with increased safety.

It would be desirable to estimate terrain parameters on-line (i.e., while the rover travels), to allow the rover to adapt to changing conditions. This could be accomplished using parameter estimation techniques [3,4]. However, these methods often rely on a closed-form analytical expression relating system inputs to the parameters of interest (e.g., equations relating rover wheel torques and velocities to terrain cohesion and internal friction angle). The complexity of classical wheel–terrain interaction equations prohibits the formulation of closed-form analytical expressions, which makes it difficult to develop on-line terrain parameter estimation algorithms. Thus, we would like to develop a simplified yet accurate form of wheel–terrain interaction equations.

Off-line parameter estimation of Martian soil has previously been performed by the Viking landers and the Sojourner and MER rovers [5,6]. The Viking landers used manipulator arms to conduct trenching experiments. The Sojourner and MER rovers used the rover wheel as a bevameter-type device to identify soil cohesion and internal friction angle. However, neither of these were on-line methods, since both missions used visual cues and off-line analysis techniques to compute soil parameters. Thus, terrain parameter information was not available to enhance the rover’s mobility and ability to conduct important scientific tasks on-line.

Here, a simplified, closed-form version of the basic mechanics of a driven rigid wheel on deformable terrain is formulated. The simplification is based on the observation that the shear and normal stress distributions beneath a driven rigid wheel can be approximated by linear functions for a wide range of terrain. Analytical comparison of the original and simplified equations is presented, and are shown to closely agree. This approach allows the formulation of an on-line terrain parameter estimation algorithm. Note that a similar approach has been used to develop an on-line parameter estimation method, with good results [4]. Experimental results from a single-wheel testbed operating in dry sand shows that the simplified equations can be used for mobility prediction with good accuracy for low-cohesion, granular soils. This method can potentially be applied to planetary exploration rovers, since much planetary terrain of interest (e.g., Martian terrain) is known to have low cohesion [6].

2. Analytical background

The interaction mechanics of a rigid wheel on deformable terrain has been studied by many researchers [7–9]. Using the Bekker formulation, the shear stress σ and normal stress τ acting on a point along a wheel rim can be expressed as (see Fig. 1):

$$\sigma(z) = (k_1 + k_2 b) \left(\frac{z}{b} \right)^n, \quad (1)$$

$$\tau(z) = (c + \sigma \tan \phi) (1 - e^{-j/k}), \quad (2)$$

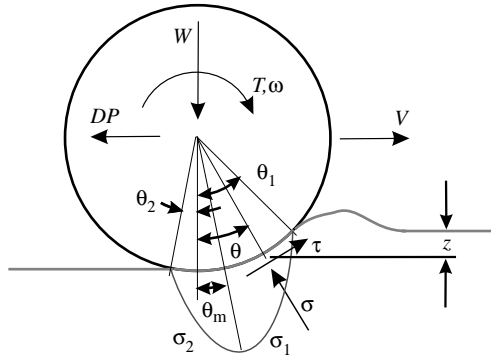


Fig. 1. Free body diagram of a driven rigid wheel on deformable soil.

where z is the wheel sinkage, n is the sinkage exponent, k_1 and k_2 are pressure sinkage moduli, b is the wheel width, j is shear deformation distance, ϕ is internal friction angle, k is the shear deformation modulus, and c is the soil cohesion. The normal stress distribution, Eq. (1), can be expressed as a function of the angular location on the wheel rim, θ , since there is a unique relationship between z , θ , and the wheel radius r :

$$\sigma_1(\theta) = (k_1 + k_2b) \left(\frac{r}{b}\right)^n (\cos \theta - \cos \theta_1)^n, \quad (3)$$

$$\sigma_2(\theta) = (k_1 + k_2b) \left(\frac{r}{b}\right)^n \left[\cos \left(\theta_1 - \frac{\theta}{\theta_m} (\theta_1 - \theta_m) \right) - \cos \theta_1 \right]^n, \quad (4)$$

where θ_m is the angular location of the maximum normal stress.

Here, the stress distribution has been divided into two zones, denoted σ_1 and σ_2 (see Fig. 1). The normal stress around the wheel rim starts from zero at the free surfaces, and increases toward a maximum value. Note that θ_m is a function of the wheel slip, i , and can be expressed as [10]

$$\theta_m = (c_1 + c_2i)\theta_1, \quad (5)$$

where c_1 and c_2 are constant coefficients.

The shear stress distribution, Eq. (2), can also be expressed as a function of the angular location on the wheel rim, by using the relationship between shear deformation distance and wheel slip [8,10]:

$$j = r[\theta_1 - \theta(1 - i)(\sin \theta_1 - \sin \theta)]. \quad (6)$$

Substituting Eq. (6) into Eq. (2) yields

$$\tau(\theta) = (c + \sigma \tan \phi) \left(1 - e^{-r/k[\theta_1 - \theta - (1-i)(\sin \theta_1 - \sin \theta)]}\right). \quad (7)$$

Force balance equations can be written for the system shown in Fig. 1 by integrating the shear and normal stress equations over the appropriate contact areas. Here we will assume $\theta_2 = 0$, since θ_2 is generally small in practice for low-cohesion

soils. The drawbar pull, DP, vertical force, W , and angular torque, T , can be computed as:

$$DP = rb \left(\int_{\theta_2}^{\theta_1} \tau(\theta) \cos \theta d\theta - \int_{\theta_2}^{\theta_1} \sigma(\theta) \sin \theta d\theta \right), \quad (8)$$

$$W = rb \left(\int_{\theta_2}^{\theta_1} \sigma(\theta) \cos \theta d\theta + \int_{\theta_2}^{\theta_1} \tau(\theta) \sin \theta d\theta \right), \quad (9)$$

$$T = r^2 b \int_{\theta_2}^{\theta_1} \tau(\theta) d\theta. \quad (10)$$

The integrals in Eqs. (8)–(10) cannot be solved analytically, due to the complex nature of the normal and shear stress equations. Thus, while numerical integration can be used to compute DP, W , and T , it is impossible to write a closed-form relationship between these forces and the terrain parameters. A closed-form relationship is required to develop an on-line terrain parameter estimation method for real-time vehicle control. This motivates the development of simplified versions of the normal and shear stress equations.

3. Model simplification

Fig. 2 shows the normal and shear stress distributions around the rim of a driven rigid wheel, for various terrain parameter values described in Table 1 [11,12]. It can be seen that the stress distributions are nearly linear. Many natural terrains have sinkage exponents n near 1 (see Eq. (3)), and thus an approximately linear stress distribution can be observed. Therefore, the normal and shear stress distribution can be approximated by linear functions. A similar observation was noted by Vincent, based on experimental studies [13].

The simplified stress equations can be written as:

$$\sigma_1(\theta) = \frac{\theta_1 - \theta}{\theta_1 - \theta_m} \sigma_m, \quad (11)$$

$$\sigma_2(\theta) = \frac{\theta}{\theta_m} \sigma_m, \quad (12)$$

$$\tau_1(\theta) = \frac{\theta_1 - \theta}{\theta_1 - \theta_m} \tau_m, \quad (13)$$

$$\tau_2(\theta) = \frac{\theta}{\theta_m} \tau_m, \quad (14)$$

where σ_m and τ_m refer to the maximum values of the normal and shear stress, respectively. These equations imply that the shear stress is very low at the free surface, which is a property of low-cohesion soils. This is acceptable, since much planetary

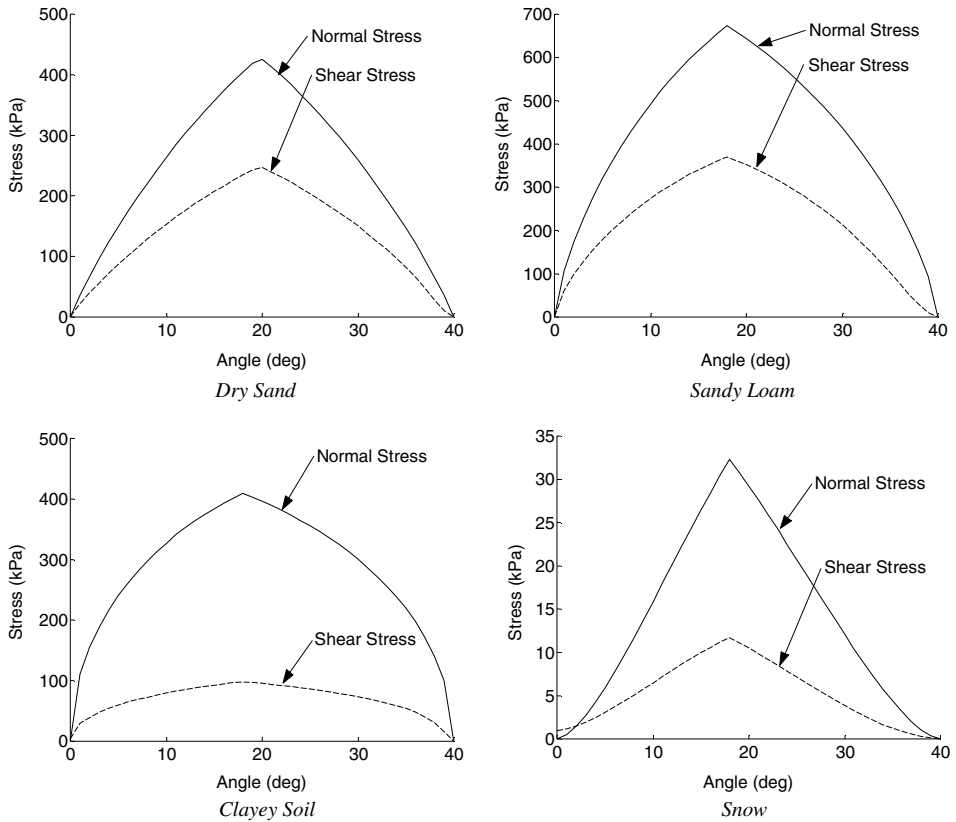


Fig. 2. Normal and shear stress distribution for various terrain types at moderate wheel slip.

Table 1
Parameters for various terrain types

	Dry sand	Sandy loam	Clayey soil	Snow
n	1.1	0.7	0.5	1.6
c (kPa)	1.0	1.7	4.14	1.0
ϕ (°)	30.0	29.0	13.0	19.7
k_c (kPa/m ^{$n-1$})	0.9	5.3	13.2	4.4
k_ϕ (kPa/m ^{n})	1523.4	1515.0	692.2	196.7
k (m)	0.025	0.025	0.01	0.04
n	1.1	0.7	0.5	1.6

terrain of interest (e.g., Martian terrain) is known to have low cohesion [6]. In practice we have found this assumption to be reasonable for soils with cohesions less than 3 kPa [14]. A simplified stress distribution for terrain with cohesion has been developed elsewhere [14].

Simulations were conducted to compare the linear approximations of the stress distribution equations (Eqs. (11)–(14)) to the original nonlinear equations (Eqs. (3), (4) and (7)). Approximately 60,000 simulations were conducted over a broad parameter space described in Table 2. These parameter ranges are reasonable for a small planetary exploration rover travelling on deformable terrain. The simulated wheel radius r was 0.072 m, and the width b was 0.033 m.

An average difference of 9.34% was found between the approximate and actual normal stress distribution equations, and 12.15% between the approximate and actual shear stress distribution equations. Thus, the linear approximations were considered sufficiently accurate representations of the true nonlinear functions.

Simplified forms of the force balance equations (Eqs. (8)–(10)) can now be written, as:

$$DP = rb \left(\int_{\theta_m}^{\theta_1} (\tau_1(\theta) \cos \theta - \sigma_1(\theta) \sin \theta) d\theta + \int_0^{\theta_m} (\tau_2(\theta) \cos \theta - \sigma_2(\theta) \sin \theta) d\theta \right), \quad (15)$$

$$W = rb \left(\int_{\theta_m}^{\theta_1} (\sigma_1(\theta) \cos \theta + \tau_1(\theta) \sin \theta) d\theta + \int_0^{\theta_m} (\sigma_2(\theta) \cos \theta + \tau_2(\theta) \sin \theta) d\theta \right), \quad (16)$$

$$T = r^2 b \left(\int_{\theta_m}^{\theta_1} \tau_1(\theta) d\theta + \int_0^{\theta_m} \tau_2(\theta) d\theta \right). \quad (17)$$

Another relation can be derived if it is assumed that the maximum shear and normal stress occur at the same point along the wheel rim:

$$\tau_m = (c + \sigma_m \tan \phi) \left(1 - e^{-k[(\theta_1 - \theta_m) - (1-i)(\sin \theta_1 - \sin \theta_m)]} \right). \quad (18)$$

The exponential term in Eq. (18) can be represented in a simplified form as

$$\tau_m = (c + \sigma_m \tan \phi) \left(1 - e^{-r/2k[(\theta_1 - \theta_m)((1+i) - (1-i) \cos \theta_1)]} \right). \quad (19)$$

Fig. 3 shows a plot of the value of the original exponential term in Eq. (18) compared to the simplified exponential term in Eq. (19) versus θ_m , for various slip ratios. The two curves closely agree, showing that the simplified exponential term

Table 2
Parameter space for algorithm analysis

Minimum value	Parameter	Maximum value
0.47	n	1.2
20.0	ϕ (°)	60.0
0.0	c (kPa)	3.0
0.0	k_1 (kPa)	140.0
520.0	k_2 (kN/m ³)	680.0
0.005	k (m)	0.04
0.0	i	1.0

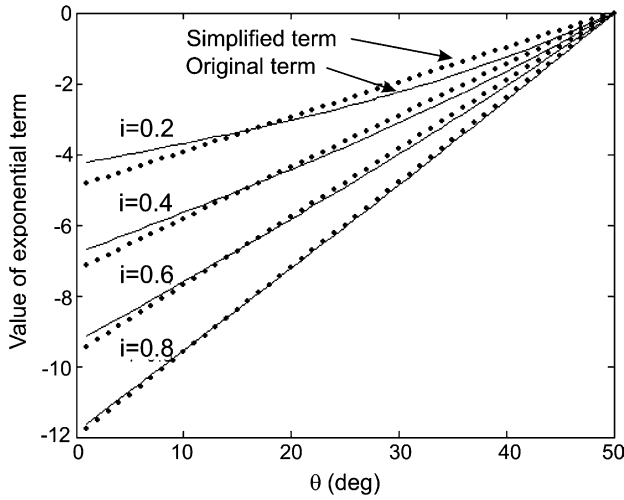


Fig. 3. Comparison of value of original exponent term and simplified term for various slip ratios.

adequately approximates the more complex original term. Simulations have been performed for various terrain parameter subsets of Table 2 to verify this.

The simplifications introduced above allow closed-form integration of the stress distribution equations, as:

$$\begin{aligned} \frac{DP}{rb} = & c \left[\frac{f}{f^2 + 1} (f \sin \theta_1 - \cos \theta_1 + e^{-f\theta_1}) \right] \\ & + \frac{1}{\theta_m(\theta_1 - \theta_m)} [(\theta_1 \cos \theta_m - \theta_m \cos \theta_1 - \theta_1 + \theta_m) \tan \phi - (\theta_1 \sin \theta_m - \theta_m \sin \theta_1)] \sigma_m \\ & - \frac{1}{\theta_m(\theta_1 - \theta_m)} \frac{1}{(f^2 + 1)^2} \left[\begin{aligned} & (f^2 - 1)(\theta_m \cos \theta_1 - \theta_1 \cos \theta_m e^{-f(\theta_1 - \theta_m)}) \\ & + 2f(\theta_m \sin \theta_1 - \theta_1 \sin \theta_m e^{-f(\theta_1 - \theta_m)}) \\ & + (f^2 - 1)(\theta_1 - \theta_m) e^{-f\theta_1} \end{aligned} \right] \sigma_m \tan \phi, \end{aligned} \tag{20}$$

$$\begin{aligned} \frac{W}{rb} = & c \left[1 - \frac{1}{f^2 + 1} (f^2 \cos \theta_1 + f \sin \theta_1 + e^{-f\theta_1}) \right] \\ & + \frac{1}{\theta_m(\theta_1 - \theta_m)} (\theta_1 \cos \theta_m - \theta_m \cos \theta_1 - \theta_1 + \theta_m) \sigma_m \\ & + \frac{1}{\theta_m(\theta_1 - \theta_m)} (\theta_1 \sin \theta_m - \theta_m \sin \theta_1) \sigma_m \tan \phi \\ & + \frac{1}{\theta_m(\theta_1 - \theta_m)} \frac{1}{(f^2 + 1)^2} \left[\begin{aligned} & -(f^2 - 1)(\theta_m \sin \theta_1 - \theta_1 \sin \theta_m e^{-f(\theta_1 - \theta_m)}) \\ & + 2f(\theta_m \cos \theta_1 - \theta_1 \cos \theta_m e^{-f(\theta_1 - \theta_m)}) \\ & + 2f(\theta_1 - \theta_m) e^{-f\theta_1} \end{aligned} \right] \sigma_m \tan \phi, \end{aligned} \tag{21}$$

$$\frac{T}{r^2 b \theta_1} = c \left(1 - \frac{1 - e^{f\theta_1}}{f\theta_1} \right) + \left[\frac{1}{2} - \frac{1}{f^2(\theta_1)^2} \frac{1}{\theta_m(\theta_1 - \theta_m)} (\theta_m - \theta_1 e^{-f(\theta_1 - \theta_m)} + (\theta_1 - \theta_m) e^{f\theta_1}) \right] \sigma_m \tan \phi, \quad (22)$$

where

$$f = \frac{r}{2k} [(1+i) - (1-i) \cos \theta_1].$$

Note that an alternative method for deriving simplified stress distribution equations is presented in [4].

These equations allow direct computation of the drawbar pull on a wheel, given knowledge of wheel load, torque, slip, sinkage, location of maximum stress, cohesion, and internal friction angle. Conversely, these equations can be solved for cohesion and internal friction angle as a function of the other variables. This implies that the cohesion and internal friction angle could be estimated by a vehicle traveling over a terrain region. (Note that this formulation might also allow estimation of a vehicle rolling resistance, as this is contained in the second term of Eq. (8).)

For practical implementation, the wheel load, torque, sinkage, slip, and location of maximum stress would need to be measured or estimated. The wheel load can be computed from a quasi-static force analysis of the rover, with knowledge of the rover configuration and mass distribution. Quasi-static analysis is valid since dynamic effects are negligible at the low speeds of planetary rovers (on the order of 10 cm/s) [1].

The torque can be estimated from the electrical current input to the motor and an empirically determined mapping from current to torque. In applications where large thermal variation is expected (such as Martian surface exploration), motor temperature can be included in this mapping [6]. Note that torque and vertical load could be directly measured if the wheel were instrumented with a multi-axis force sensor. However, this adds cost, weight and complexity to the system.

The sinkage can be computed with vision-based techniques or by kinematic analysis of the rover suspension [15,16]. The wheel angular speed can be measured with a tachometer. The wheel linear speed can be computed using inertial measurement unit (IMU) measurements, and thus slip can be computed. However, at low speeds IMU velocity measurements are degraded by noise. In this case, machine vision-based techniques such as visual odometry can yield more accurate results [17].

The location of the maximum stress can be estimated to occur at the angular location midway between the values of θ_1 and θ_2 . This assumption is reasonable for a wide range of soils at moderate slip ratios [14]. This can be justified by noting that θ_m can be estimated from Eq. (5). The range of c_1 and c_2 is generally $c_1 \approx 0.4$ and $0 \leq c_2 \leq 0.3$ [10]. Thus for a wide range of slip ratios, θ_m will be near 0.5.

In this formulation, the parameter k is assumed to be known. In practice, the estimation algorithm exhibits low sensitivity to k , particularly for large wheel radii and high slip ratios. Therefore k is usually chosen as a representative value for deformable terrain. Techniques for estimating k are described in [14].

The sensors described above (i.e., rover configuration sensors, motor current sensor, wheel tachometer, IMU, and vision system) would likely be part of a planetary exploration rover system. Thus, all required inputs can be measured or estimated with on-board rover sensors.

4. Simulation results

Simulations of a driven rigid wheel traveling through loose sand were performed to study the accuracy of the simplified equations. The simulation parameters are shown in Table 3. The torque and drawbar pull computed from Eqs. (20) and (22) were compared to numerically integrated values of the original equations (Eqs. (8) and (10)).

Results from representative simulation trials are shown in Figs. 4 and 5. It can be seen that the simplified and original equations agree closely in predicting drawbar pull and torque. This implies that the simplified equations are reasonable representations of the original equations. The average percent difference was 2.0% for drawbar pull and 2.6% for torque.

5. Experimental results

Experiments were performed to evaluate the simplified equations' ability to predict forces on a rigid wheel in dry sand. The experimental testbed consists of a driven rigid wheel mounted on an undriven vertical axis (see Fig. 6) [14]. The wheel assembly is mounted to a pulley driven horizontal carriage. By driving the wheel and carriage at different rates, variable slip ratios can be imposed. The vertical wheel load can be changed by adding weight to the vertical axis.

The testbed is instrumented with encoders to measure angular velocities of both the wheel and the carriage pulley. The carriage linear velocity is computed from the carriage pulley angular velocity. The vertical wheel sinkage is measured with a linear potentiometer. The drive motor current is estimated by measuring the voltage across a current-sense resistor. The six-component wrench between the wheel and carriage

Table 3
Simulation parameters for loose sand

Parameter	Value
n	1.15
ϕ (°)	31.0
c (kPa)	0.7
k_1 (kPa)	0.0
k_2 (kN/m ³)	520.0
k (m)	0.04
i	0.3
r (m)	0.08
b (m)	0.03

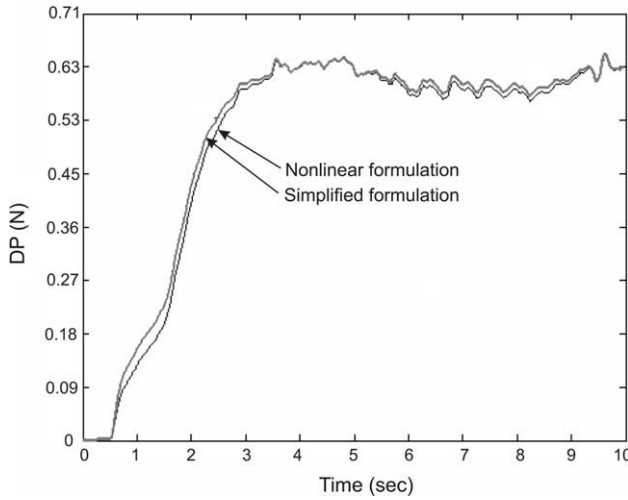


Fig. 4. Comparison of original drawbar pull and simplified formulation.

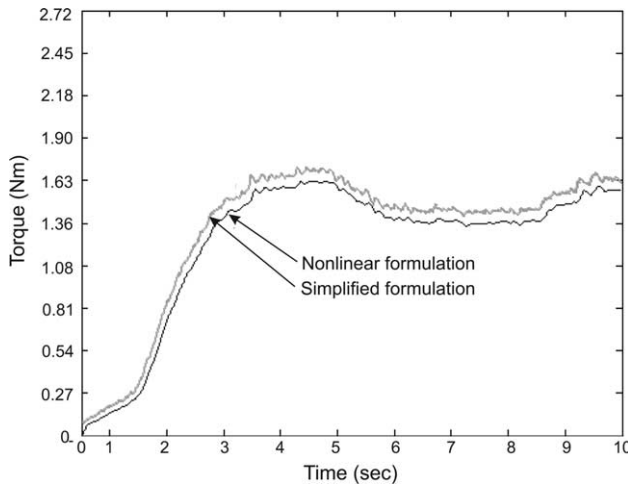


Fig. 5. Comparison of original torque and simplified formulation.

is measured with an six-axis force/torque sensor. The force sensor allows measurement of the normal load W and drawbar pull DP . The prediction algorithm is run on an Intel 486 66 MHz processor at a rate of 250 Hz.

The wheel radius and width were 0.072 and 0.071 m, respectively. The wheel maximum angular velocity is 1.1 rad/s. This results in a maximum linear velocity of 0.080 m/s, which is the maximum carriage velocity. The wheel size and speed were chosen to be similar to projected planetary rovers.

Drawbar pull and torque was recorded while the wheel was driven under various loads, at various slip ratios. This data was compared to values of drawbar pull and

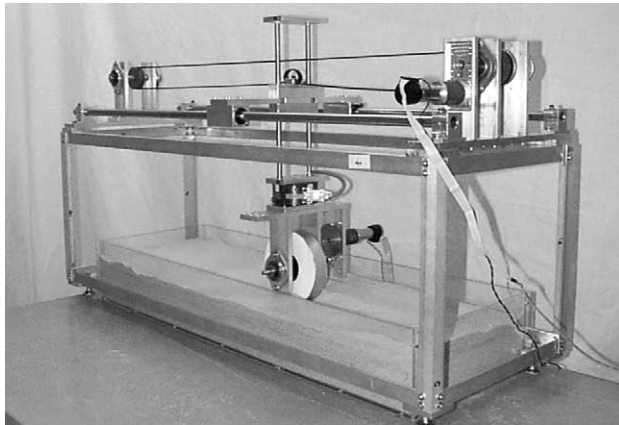


Fig. 6. Terrain characterization testbed.

torque computed from the simplified equations (Eqs. (20) and (22), respectively), and to numerically integrated values of the original equations (Eqs. (8) and (10), respectively). The terrain parameters c , ϕ , and k , were determined by external measurement using a bevameter.

Representative results can be seen in Figs. 7 and 8. The predicted values agree closely with experimentally measured results. For drawbar pull (Fig. 7) the average percent difference between the experimentally measured value and the nonlinear formulation is 21.2%, and 13.4% for the simplified formulation. The standard deviation of the difference was 8.5% for the nonlinear formulation and 7.0% for the

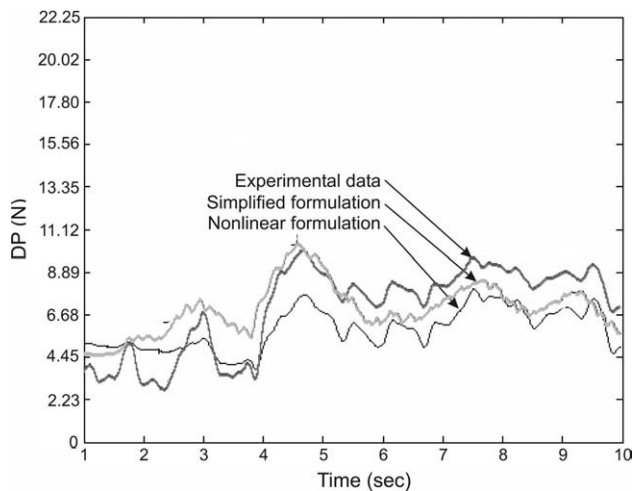


Fig. 7. Comparison of drawbar pull prediction from original equation, simplified equation and experimental data.

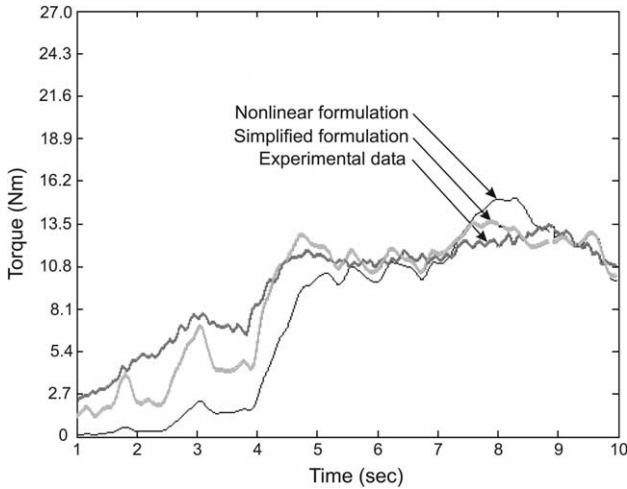


Fig. 8. Comparison of torque prediction from original equation, simplified equation and experimental data.

linear formulation. For torque (Fig. 8) the average percent difference between the experimentally measured value and the nonlinear formulation is 16%, and 15% for the simplified formulation. The standard deviation of the difference was 12.2% for the nonlinear formulation and 9.4% for the linear formulation.

Differences between experimental and predicted data were likely due to terrain inhomogeneity or wheel dynamic forces, since these effects are not considered in the analysis. Sensor noise on the force, wheel velocity, and sinkage measurements also introduced error into the experimental measurements. Overall, however, these results show that the simplified equations can be used for wheel–terrain interaction force prediction with reasonably good accuracy. This suggests that they could be used as a basis for a terrain parameter estimation method. This is a focus of current research. A similar approach to the one presented here has successfully been used to develop an on-line parameter estimation method, with good results [4].

6. Conclusions

A simplified, closed-form version of the basic mechanics of a driven rigid wheel on deformable terrain has been presented. These equations allow the formulation of an on-line terrain parameter estimation algorithm, which is important for vehicles such as planetary exploration rovers. Analytical comparisons of the original and simplified equations were presented and shown to closely agree, implying the simplified equations are adequate representations of the complex original equations for a range of soil types. Experimental results from a single-wheel testbed operating in dry sand show that the simplified equations can be used for mobility prediction with good accuracy.

Acknowledgement

This work was supported by the NASA Jet Propulsion Laboratory.

References

- [1] Weisbin C, Rodriguez G, Schenker P, Das H, Hayati S, Baumgartner E, et al. Autonomous rover technology for mars sample return. In: Proceedings of the international symposium on artificial intelligence. Robotics and Automation in Space; 1999.
- [2] Bekker G. Introduction to terrain–vehicle systems. Ann Arbor: University of Michigan Press; 1969.
- [3] Koch K. Parameter estimation and hypothesis testing in linear models. Berlin: Springer; 1988.
- [4] Iagnemma K, Shibly H, Dubowsky S. On-line terrain parameter estimation for planetary rovers. In: Proceedings of IEEE international conference on robotics and automation; 2002.
- [5] Moore H, Hutton R, Scott R, Spitzer C, Shorthill R. Surface materials of the Viking landing sites, Mars. *J Geophys Res* 1977;82(28).
- [6] Matijevic J, Crisp J, Bickler D, Baner R, Cooper B, Eisen H, et al. Characterization of Martian surface deposits by the Mars pathfinder rover, Sojourner. *Science* 1997;278(5):1765–8.
- [7] Bekker G. Theory of land locomotion, the mechanics of vehicle mobility. Ann Arbor: The University of Michigan Press; 1956.
- [8] Onafko O, Reece R. Soil stresses and deformation beneath rigid wheels. *J Terramech* 1967;4(1):59–80.
- [9] Plackett C. A review of force prediction methods for off-road wheels. *J Agri Eng Res* 1985;31:1–29.
- [10] Wong J, Reece A. Prediction of rigid wheel performance of driven rigid wheels, Part I. *J Terramech* 1967;4(1):81–98.
- [11] Yong R, Fattah E, Skiadas N. Vehicle traction mechanics. Amsterdam: Elsevier Science Publishers; 1984.
- [12] Wong J. Terramechanics and off-road vehicles. Amsterdam: Elsevier Science Publishers; 1989.
- [13] Vincent E. Pressure distribution on and flow of sand past rigid wheel. In: Proceedings of the first international conference on terrain–vehicle systems; 1961. p. 859–77.
- [14] Kang S. Terrain parameter estimation and traversability assessment for mobile robots. MS thesis. Massachusetts Institute of Technology, Cambridge; 2003.
- [15] Iagnemma K, Kang S, Brooks C, Dubowsky S. Multi-sensor terrain estimation for planetary rovers. In: Proceedings of the seventh international symposium on artificial intelligence. Robotics and Automation in Space, i-SAIRAS; 2003.
- [16] Wilcox B. Non-geometric hazard detection for a mars microrover. In: Proceedings of the AIAA conference on intelligent robotics in field, factory, service, and space, vol. 2; 1994.
- [17] Olson C, Matthies L, Schoppers M, Maimone M. Stereo ego-motion improvements for robust rover navigation. In: Proceedings of the IEEE international conference on robotics and automation; 2001.